Chapter 3

PHOTO-TRIGGERED ELECTRON TRANSFER THROUGH TRYPTOPHAN IN RU-P450 SYSTEMS

3.1. Background: Light to ET

To accomplish metabolic processes that drive biological function, cells must deliver electrons and holes over many-angstrom distances, and generate highly reactive species in a very controlled manner. The photosynthetic reaction center in plants is a paradigm in its ability to harness the energy in sunlight to produce high-energy states that can rapidly and efficiently separate charges (electrons and holes) over greater than 20 Å. This allows use of the reactive electrons to generate reduced nicotinamide adenine dinucleotide (phosphate) (NAD(P)H) and adenosine triphosphate (ATP) (the energy currency of the cell), and sequestration of the reactive holes to oxidize water and generate molecular oxygen.

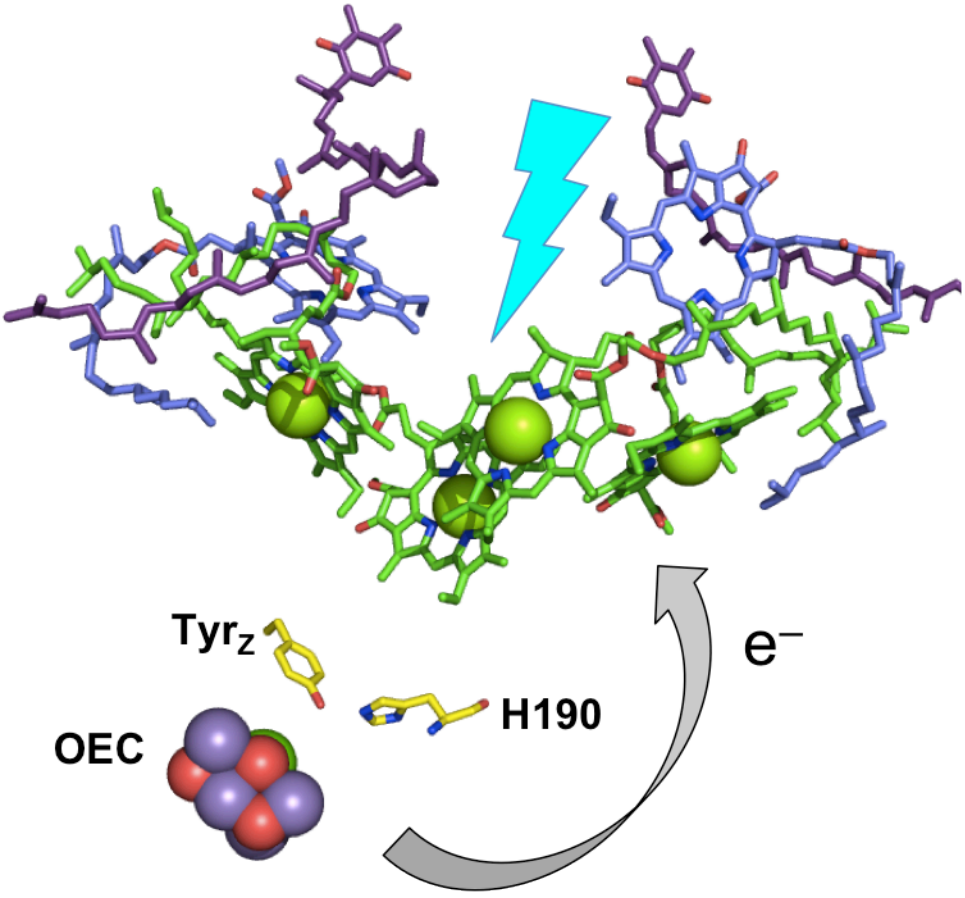

Figure 3.1. Photo-excitation of P680 chromophores in Photosystem II triggers oxidation of the oxygen evolving complex (OEC).

As described in Chapter 2, we have developed a ruthenium photosensitizer/cytochrome P450 BM3 conjugate system (**Figure 3.2**) that similarly harnesses light energy (a laser pulse) to photochemically oxidize the P450 active site by one electron.[1] We have generated the high-valent heme-hydroxo species known as compound II (CII) by oxidizing an axially-bound water molecule (**Figure 3.3**). This is the first step in running cytochrome P450 backwards to access the highly-reactive, iron-oxo ligand radical intermediate known as compound I (CI).

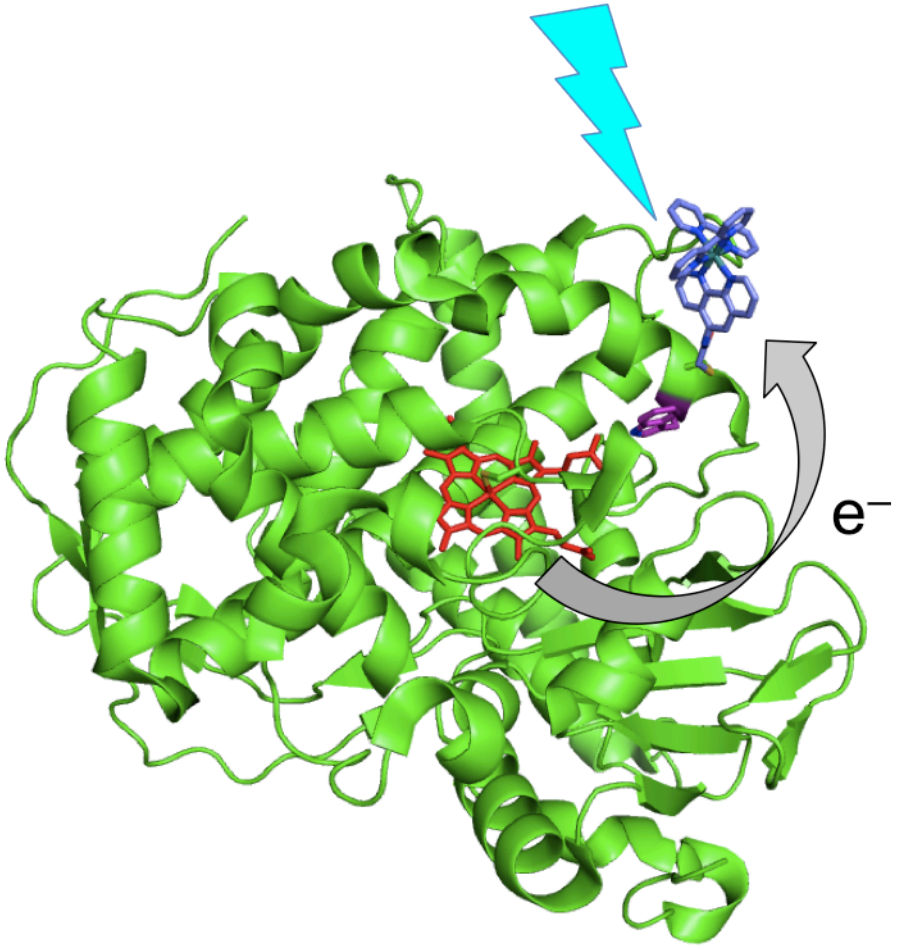

Figure 3.2. Photo-excitation of the tethered ruthenium complex triggers oxidation of the P450 heme active site. The photosensitizer (Ru^{II}(2,2′-bipyridine)$_2$(5-acetamido-1,10-phenanthroline)) is highlighted in blue, the heme is red, and intervening tryptophan 96 is colored purple.

CI is capable of hydroxylating unactivated alkane C–H bonds, a critical transformation in the biosynthesis of steroids, among many other cellular processes. This reactive species has been chemically generated by rapid mixing of *m*CPBA (*meta*-chloroperoxybenzoic acid with the thermophilic P450 CYP119.[2] However, the processes of hydrogen atom abstraction from substrate to form CII, and subsequent radical rebound to generate hydroxylated product and regenerate the resting state, have yet to be observed directly. The rate of formation of CI is often slower than that for its reaction with substrate.[3] Photochemical oxidation of the active site provides a rapid means of generating these oxidized species, with very high temporal resolution.

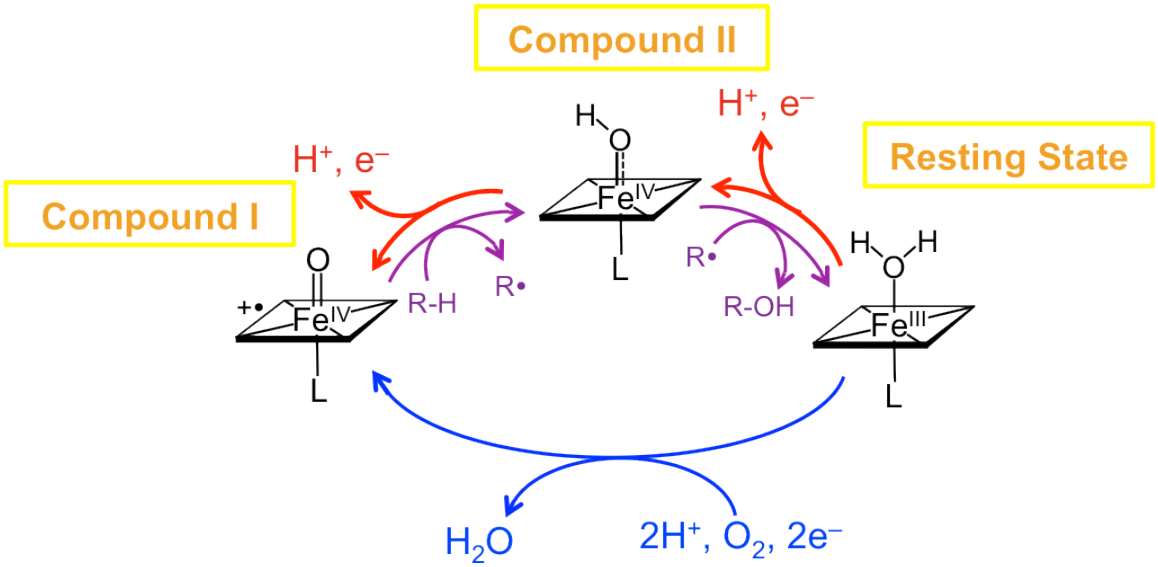

Figure 3.3. Formation of high-valent CI and CII. Blue arrows: reductive activation of dioxygen (native catalytic cycle). Red arrows: oxidative activation of water. Purple arrows: hydroxylation of substrate (RH).

Generation of CI requires two-electron oxidation of the heme (**Figure 3.3**, red arrows). If we wish to achieve, observe, and characterize this second electron transfer by photochemical oxidation (flash-quench), we need to first obtain a stable pool of the precursor CII. Photochemically generated CII decays within a

few hundred milliseconds. Additionally, the yield of this species low; rough estimates place this yield at less than 20%, based on the observed transient absorption features (Chapter 2), and reported absorption profile of CII species in chloroperoxidase (a related, thiolate-ligated heme enzyme) and P450.[4,5] Thus, it would be extremely challenging to observe photochemical generation of CI via two sequential rounds of flash-quench, much less characterize the reaction of this active hydroxylating species with substrate.

Instead, if we can generate CII by chemical means with sufficient yield and purity, we may be able to photo-trigger the second oxidation step. The rigorous purification that can be achieved for thermo-stable CYP119 has been cited as the most critical aspect for chemical oxidation to CI in high yield.[6] If we can extend our photochemical system to CYP119, we anticipate that one-electron *chemical* oxidation followed by one-electron *photochemical* oxidation will form CI.

If we wish to use flash-quench to generate observable yields of CI, we also must gain a better understanding of the factors affecting the rate and yield of photochemical heme oxidation. The rate constant for heme oxidation to the porphyrin radical ($Fe^{III}(OH_2)P^{\bullet+}$) is k = 8x10^5 s^{-1} at pH 8.[1] This rate is similar to that observed for heme systems containing a direct, covalent linkage between the photosensitizer and the porphyrin framework,[7] suggesting that a favorable coupling pathway connects the photosensitizer and heme in our Ru-P450 conjugate.

The intervening protein medium between electron donor and acceptor influence the efficiency of ET over long distances; this is discussed in more detail in Chapter 4. In particular, aromatic amino acid residues can participate as redox intermediates in multi-step ET, or electron "hopping."[8–10] Tryptophan is a redox

intermediate in photo-triggered electron hopping in a rhenium-modified blue copper protein, *Pseudomonas aeruginosa* azurin (**Figure 3.5**). The electronically excited rhenium carbonyl complex transiently oxidizes a nearby tryptophan, which in turn oxidizes the copper center.[8] This multistep reaction accelerated the overall copper oxidation event by two orders of magnitude compared to single step ET tunneling over the same distance.

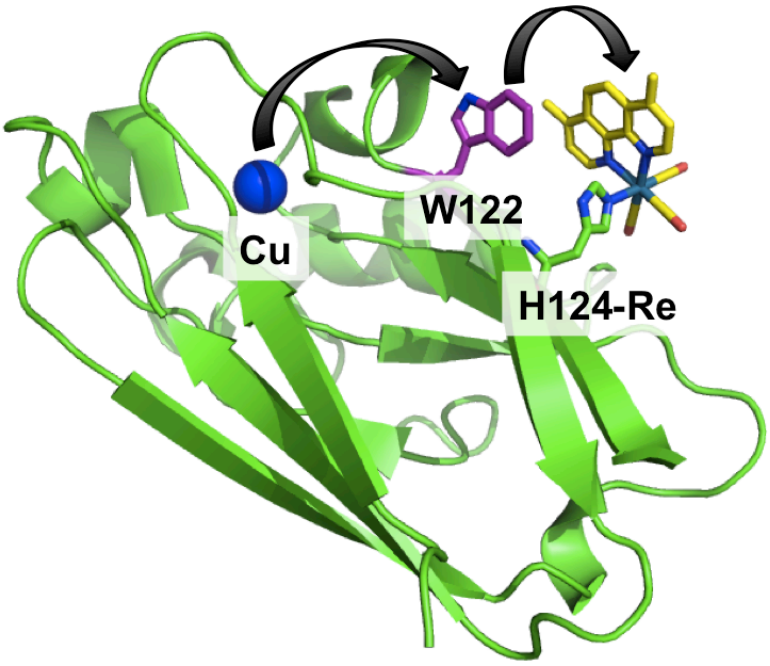

Figure 3.4. Multistep ET in rhenium-labeled azurin. Black arrows indicate the two ET steps that oxidize the protein metal center.

We noted that the photosensitizer tethering position in our Ru-P450$_{BM3}$ conjugate is directly adjacent to tryptophan 96, which forms hydrogen bonds with a heme propionate. We have hypothesized that this intervening tryptophan facilitates hole transfer to the heme (**Figure 3.5**), in analogy to work on azurin.

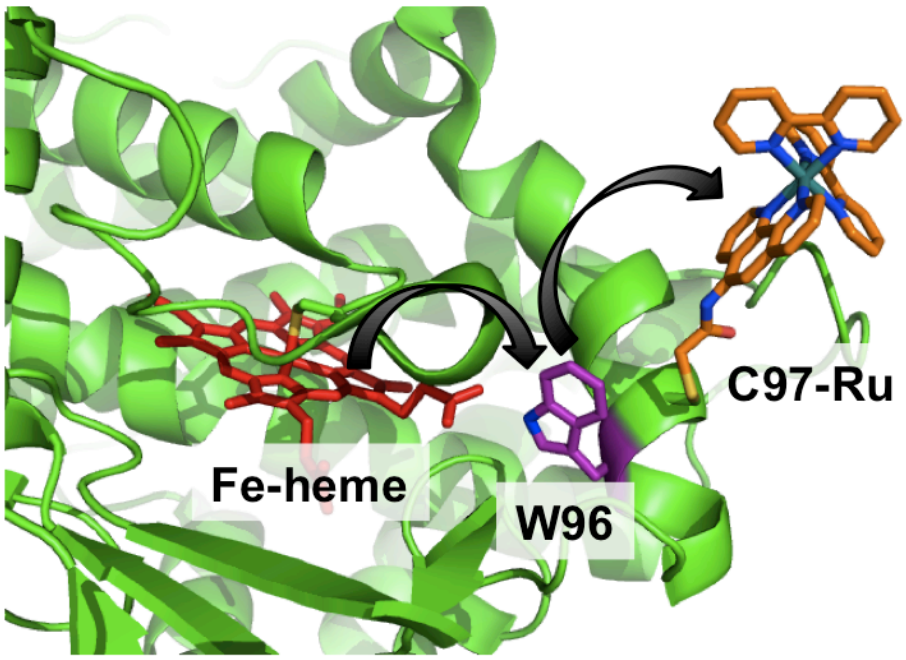

Figure 3.5. Multistep ET in ruthenium-labeled cytochrome P450. Black arrows indicate the two ET steps that oxidize the protein metal center.

This Chapter describes our efforts to probe the role of W96 in the photochemical heme oxidation of Ru_{C97}-P450 BM3, and to engineer a similar system that will allow photo-triggered oxidation of the CYP119 active site, with the aim of photochemical production of compound I in this thermostable enzyme.

3.1.1. P450 systems: Motivation and selection

The functional photochemical system in P450 BM3 (Chapter 2) involves a triple mutant of the heme domain, which will be abbreviated as C97-BM3(W). Two native surface-exposed cysteines were removed (C62A/C156S) and a single cysteine added (K97C) to achieve selective, covalent conjugation of the photosensitizer [Ru(2,2′-bipyridine)$_2$(5-iodoacetamido-1,10-phenanthroline)]$^{2+}$ (Ru^{II}(bpy)$_2$(IAphen)) directly adjacent to W96 (**Figure 3.6**).

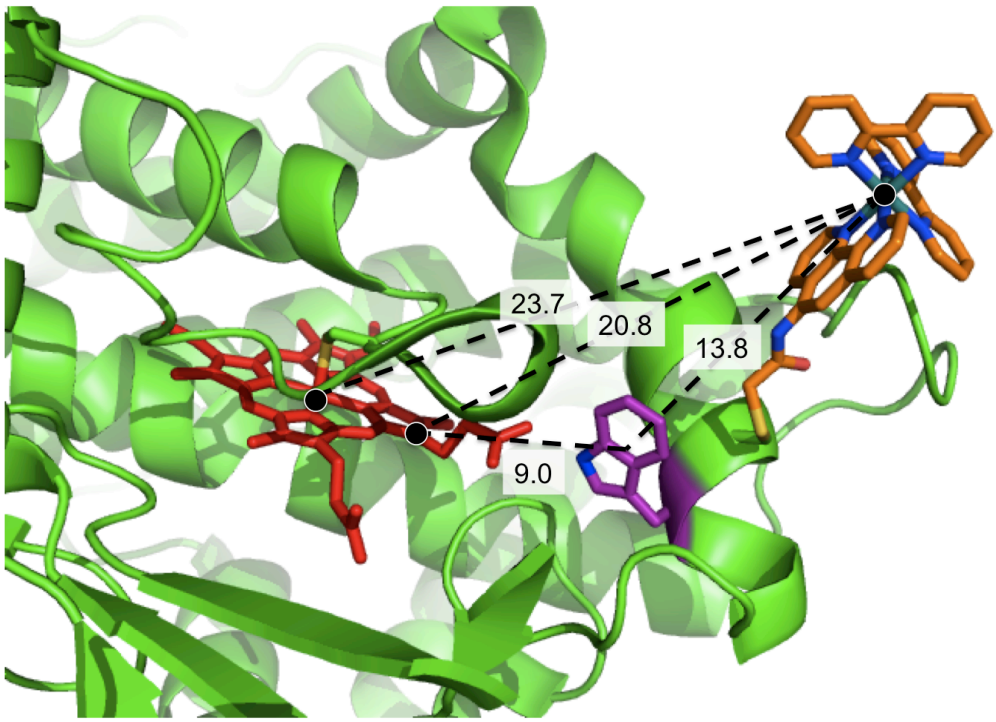

Figure 3.6. Putative multistep ET pathway in Ru_{C97}-BM3(W). Residue W96 forms hydrogen-bond contacts with the heme propionates (2.7, 3.5 Å). Highlighted distances are: Ru-Fe (23.7 Å), Ru-porphyrin edge (20.8 Å), Ru-W(centroid) (13.8 Å), W(centroid)-Fe (12.9 Å), W(centroid)-edge of pyrrole (9.0 Å).

To probe the role of this intervening tryptophan, we have generated the quadruple "W-negative" mutant: C62A/C156S/K97C/W96H, abbreviated C97-BM3($_W$H). Note that the subscript refers to the native residue, in this case, tryptophan. This mutation is expected to preserve hydrogen-bonding with the heme propionates, an aspect that is thought to provide structural stability to the heme.[11] More importantly, this mutation will act as a control in which multistep electron transfer is not expected to occur. The $His^{\bullet+}$/His reduction potential ($E°$ = 1.5 V vs. NHE, phosphate buffer pH 8) is much higher than the analogous $Trp^{\bullet+}$/Trp potential ($E°$ = 0.98 V vs. NHE, phosphate buffer pH 8).[12] The $Ru^{III/II}$ reduction potential is approximately 1.3 V vs. NHE.[13,14] Oxidation of histidine would be thermodynamically *uphill* by 200 mV, whereas oxidation of tryptophan has a

driving force of approximately 300 mV. If this W96 is indeed involved in multistep electron transfer, we would expect the W96H mutation to drastically impair photochemical heme oxidation by Ru^{III} oxidants.

Alternatively, this tryptophan could act as a sink for electron holes, sequestering the oxidizing equivalents away from the heme and lowering the yield of compound II formation. Chemical oxidation of P450-cam from *Pseudomonas putida* and P450-BM3 by oxygen donors (hydrogen peroxide, peroxyacids) has been shown to result in formation of a so-called "compound ES", a ferryl species in which one oxidizing equivalent had been transferred to an amino-acid side chain near the heme – either tryptophan or tyrosine.[15,16] If this is the case for our photochemical system, we would anticipate that the W96H mutation would actually *increase* the observed rate and yield of heme oxidation.

To develop a photochemical system in CYP119, we chose to mimic Ru-P450-BM3 as closely as possible. In the slightly smaller, more compact CYP119 (**Figure 3.7**), the only native cysteine residue is C317; this residue is buried within the protein active site, and provides critical thiolate ligation to the heme. Therefore, a single mutation is sufficient to achieve selective photosensitizer conjugation. In the native structure of CYP119, H76 forms hydrogen bonds to the CYP119 heme propionates, analogous to W96 in P450 BM3. The adjacent residue is D77 (analogous to K97), and we have mutated this to cysteine to allow photosensitizer conjugation (**Figure 3.8**). This mutant will be abbreviated C77-CYP119(H).

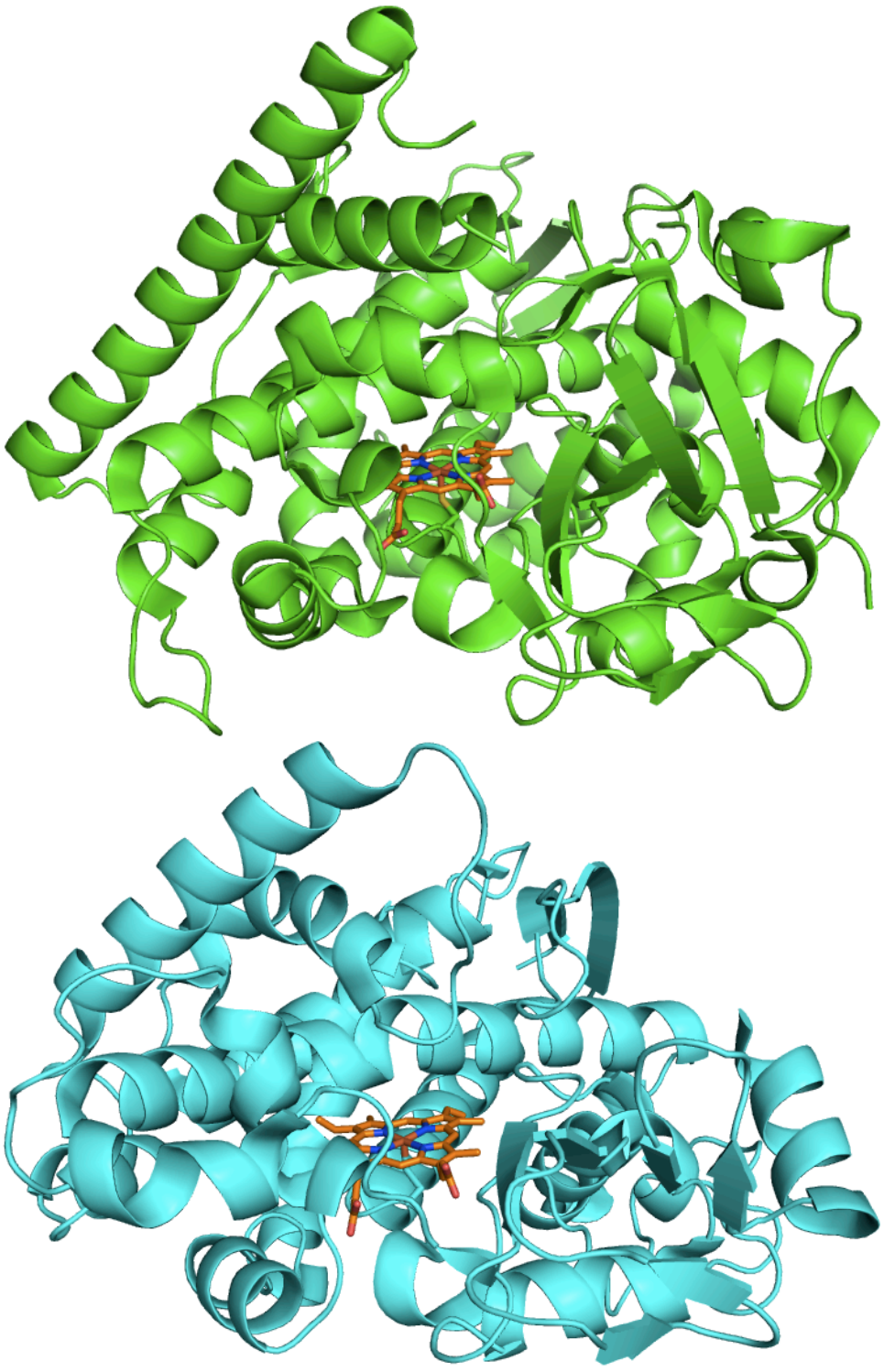

Figure 3.7. Structures of P450 BM3 (top, green. PDB: 2IJ2) and CYP119 (bottom, cyan. PDB 1IO7).

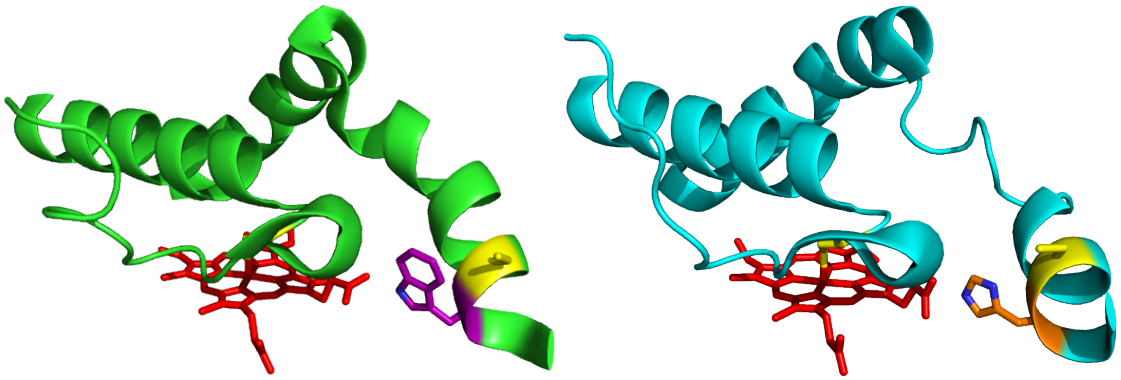

Figure 3.8. Photosensitizer conjugation sites in P450-BM3 (left, green) and CYP119 (right, cyan) are highlighted in yellow.

As discussed for the P450-BM3 systems, we wish to probe the role of tryptophan in assisting or impeding electron transfer. With this goal in mind, we will also generate a tryptophan-containing CYP119 double mutant D77C/H76W. This mutant is abbreviated as C77-CYP119($_{H}$W); note, again, that the subscript denotes the native residue.

3.2. Results and Analysis

3.2.1. Characterization of mutants

It is possible that a seemingly-insignificant mutation can have large effects on protein stability and structure. It is critical to verify that there are no observable changes in structure or stability of the mutants. The three mutants have been characterized by UV-visible absorption, and mass spectrometry. Crystals were obtained for the C97-BM3($_{W}$H) mutant, and the crystal structure was determined.

UV-visible absorbance

All of the P450 mutants have strong Soret absorbances near 420 nm, and Q-band features in the 500-600 nm range. The P450-BM3 mutants have a Soret maximum at 418 nm, while both CYP119 mutants have a Soret maximum at 416 nm (**Figure**

3.9). The Soret maximum is very sensitive to environment, including changes in buffer composition and protein purity. Therefore, small changes in absorbance must be assessed with care. The origin of the discrepancy in absorbance between C97-BM3($_{W}$H) and the other three mutants has not been determined.

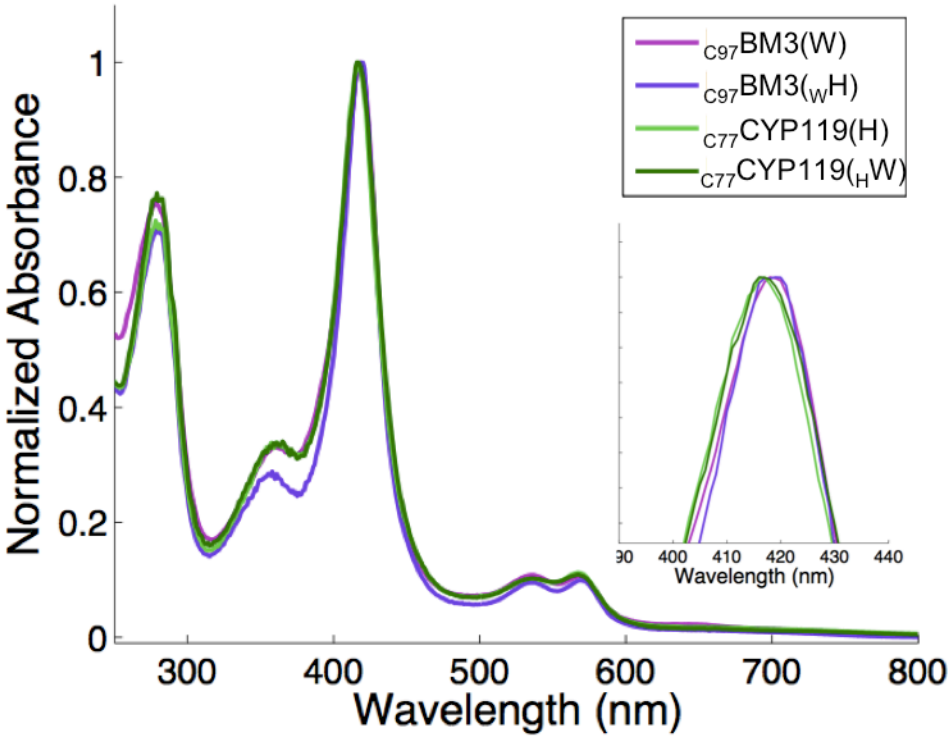

Figure 3.9. UV-visible absorbance spectra of P450 mutants. C97-BM3(W) (magenta), C97-BM3($_{W}$H) (purple), C77-CYP119(H) (light green), C77-CYP119($_{H}$W) (dark green).

X-ray crystal structure analysis of C97-BM3($_{W}$H)

The crystal structure of C97-BM3($_{W}$H) has been determined with 2.2 Å resolution. Two monomers were found in the asymmetric unit. The C97-BM3($_{W}$H) structure overlays very well with WT P450 BM3 in the open, substrate-free form (pdb: 2IJ2, RMSD = 0.277). C97-BM3($_{W}$H) overlays significantly less well with the closed, substrate-bound form (2UWH, RMSD = 0.666) (**Figure 3.10**). This is in contrast

to the crystal structure of Ru_{C97}-BM3(W), which crystallized in the open form, with an unidentified substrate in the pocket.

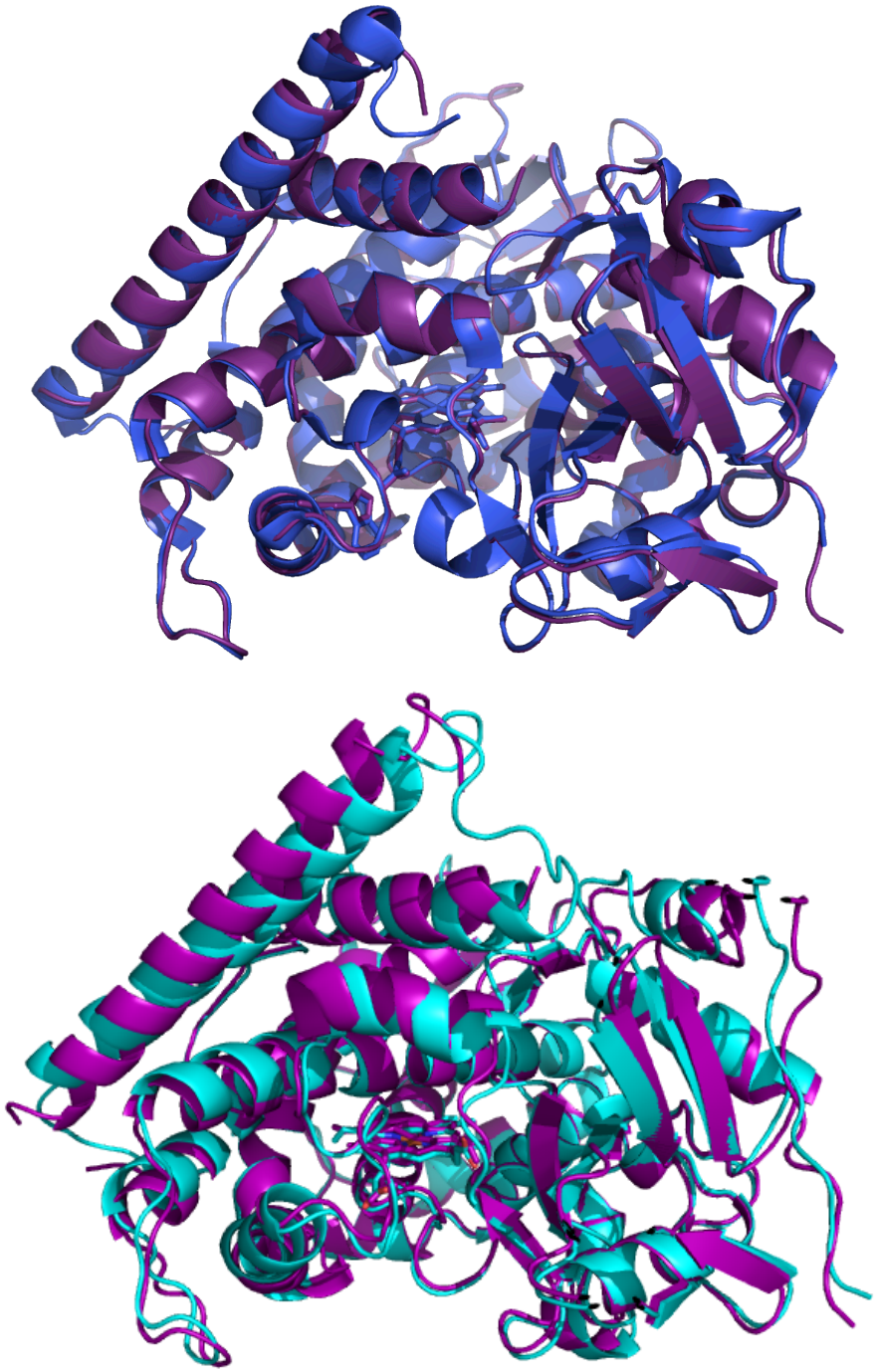

Figure 3.10. Overlay of C97-BM3($_{W}$H) (purple) with open and closed WT BM3 structures. **Top**: Open form (blue). **Bottom**: Closed form (cyan).

Electron density clearly shows the W96H mutation (**Figure 3.11**). H96 is within hydrogen-bond distance of the heme propionate (2.8 and 4.4 Å between His96 Nε and the two propionate oxygen atoms, respectively). The position of this residue overlays almost exactly with the indole moiety of W96 in the wild-type structure.

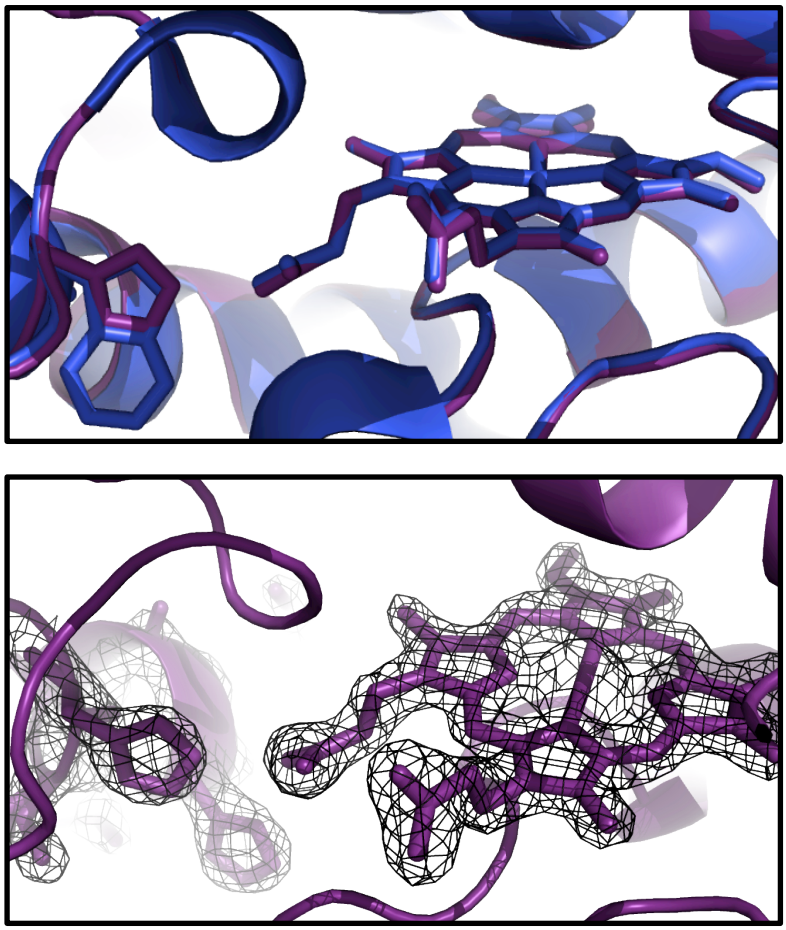

Figure 3.11. C97-BM3($_{W}$H) active site. **Top**: Overlay of C97-BM3($_{W}$H) (purple) with WT P450 BM3 (PDB: 2IJ2, blue), highlighting the overlay of W96 and H96 residues. **Bottom**: Electron density map showing H96 within hydrogen bond contact of the heme propionates.

Based on comparison of the C97-BM3($_{W}$H) structure to that of WT P450 BM3, it appears that this single mutation has no significant effect on the structure. We anticipate that possible changes in rate or yield of heme oxidation are a direct

result of the tryptophan-to-histidine substitution, and not to other structural perturbations.

3.2.2. Ru-P450 Luminescence

Steady state and transient luminescence spectroscopies were used to probe the nature of the photosensitizer conjugated to the P450 surface. When excited with blue light (e.g., 480 nm), the steady-state spectrum of all Ru-P450 conjugates closely resembles those of the free photosensitizer [Ru^{II}(2,2′-bipyridine)$_2$(5-acetamido-1,10-phenanthroline)]$^{2+}$ ([Ru(bpy)$_2$(A-phen)]$^{2+}$) and [Ru(bpy)$_3$]$^{2+}$ (see Chapter 2 for an example). None of the unlabeled P450 mutants show detectable luminescence.

Luminescence decays and exponential fits of all four Ru-P450 conjugates are shown in **Figure 3.13**. Lifetimes for all four mutants are reported in **Table 3.1**. As discussed in Chapter 2, the Ru^{II}_{C97}-BM3(W) excited state decay is biexponential, with approximately 65% of a 200 ns decay component, and 35% of a 50 ns decay component. We interpreted this observation as two different conformations of the photosensitizer that do not exchange on the timescale of this measurement. In the presence of quencher, the luminescence lifetime is dramatically reduced, and can be approximated by a monoexponential decay with lifetime of 30 ns.

The other mutants show similar luminescence decays, with minor differences. The histidine-containing mutants (Ru^{II}_{C97}-BM3($_W$H) and Ru^{II}_{C77}-CYP119(H) are nearly monoexponential. As is evident from the overlays (**Figure 3.14**), there is a strong similarity in the luminescence decay of the two histidine-containing mutants (green, blue), as well as similarity between the tryptophan containing mutants (red, purple). Curiously, the excited state of Ru^{II}_{C77}-CYP119(H) is not as effectively quenched by 17 mM [Ru(NH$_3$)$_6$]$^{3+}$, in comparison to the other conjugates.

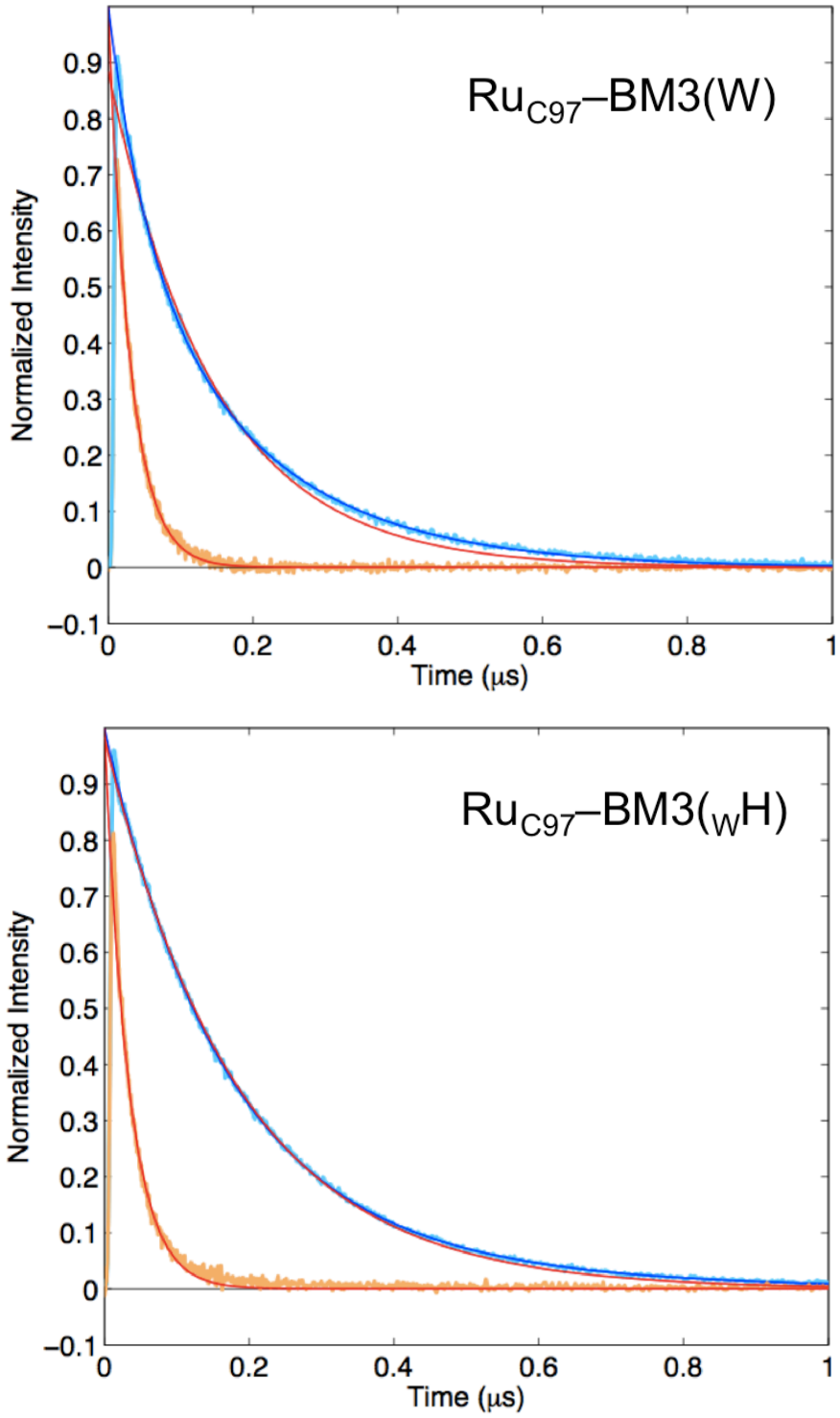

Figure 3.12. Time-resolved luminescence decays of Ru-BM3 conjugates in the presence (blue) and absence (orange) of 17 mM $[Ru(NH_3)_6]^{3+}$ quencher. Monoexponential fits are shown in red, biexponential fits are shown in dark blue. Samples were excited at 480 nm, and luminescence was detected at 630 nm.

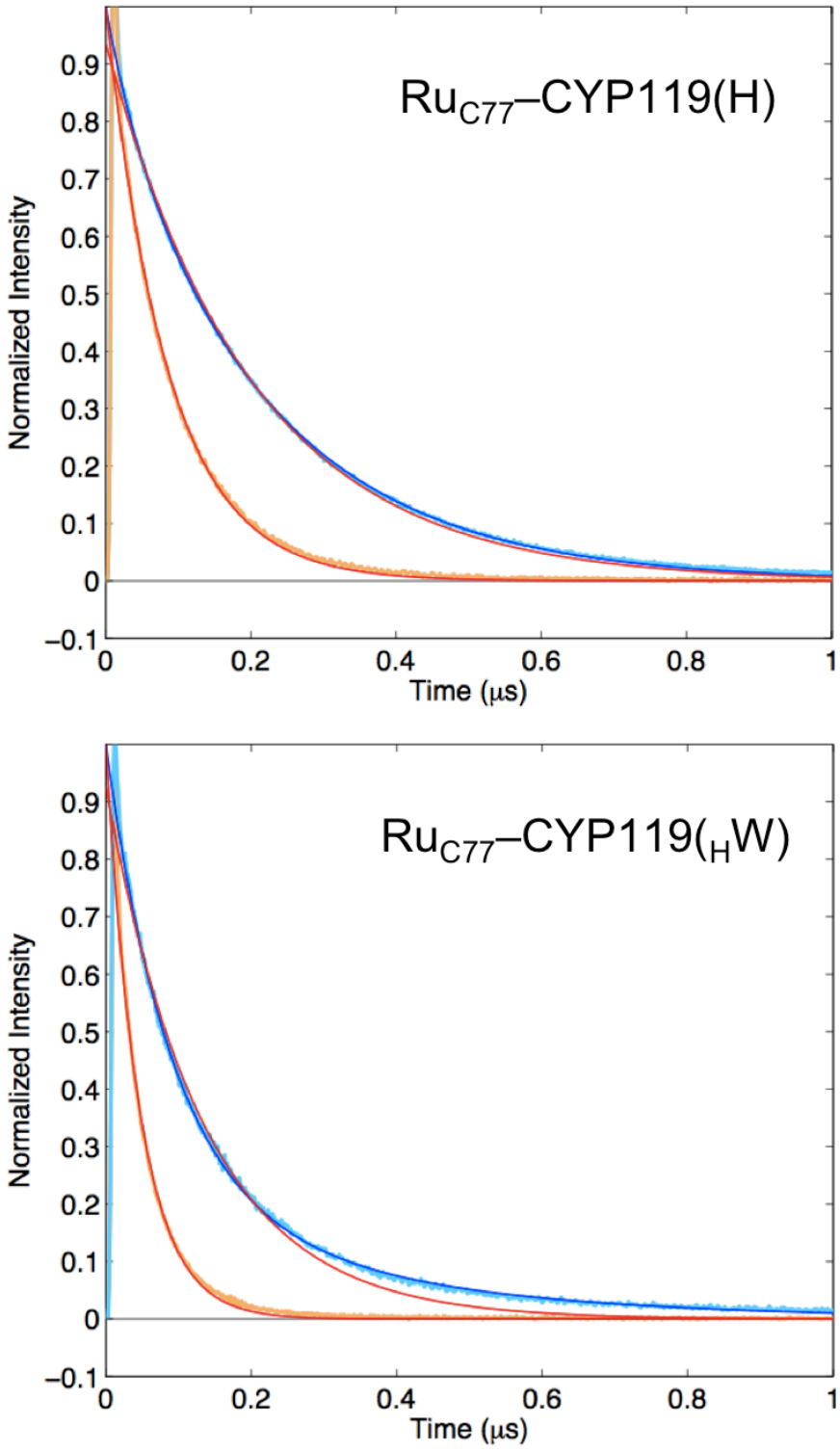

Figure 3.13. Time-resolved luminescence decays of Ru-CYP119 conjugates in the presence (blue) and absence (orange) of 17 mM $[Ru(NH_3)_6]^{3+}$ quencher. Monoexponential fits are shown in red, biexponential fits are shown in dark blue. Samples were excited at 480 nm, and luminescence was detected at 630 nm.

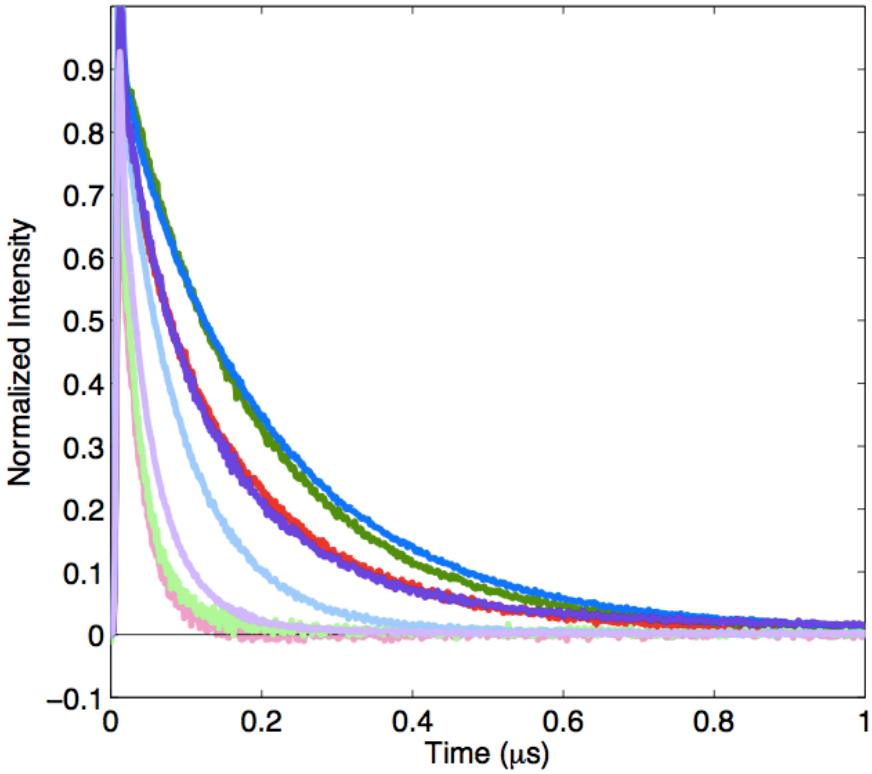

Figure 3.14. Overlay of luminescence decays for four Ru-P450 conjugates. 630 nm, in the absence (bold colors) and presence (pastels) of 17 mM $[Ru(NH_3)_6]^{3+}$ quencher. Ru^{II}_{C97}-BM3(W) (red, pink); Ru^{II}_{C97}-BM3($_W$H) (green); Ru^{II}_{C77}-CYP119(H) (blue); Ru^{II}_{C77}-CYP119($_H$W) (purple).

Table 3.1. Excited state lifetimes of four Ru-P450 conjugates in the absence and presence of 17 mM $[Ru(NH_3)_6]^{3+}$ quencher. Both major (a) and minor (b) components are listed for the biexponential fit. Samples were excited at 480 nm, and luminescence was detected at 630 nm.

Enzyme	conditions	τ_{mono}(ns)	τ_a(ns)	τ_b(ns)	%a	%b
Ru_{C97}-BM3(W)	unquenched	140	190	52	65	35
	$[Ru(NH_3)_6]^{3+}$	30				
Ru_{C97}-BM3($_W$H)	unquenched	180	160	310	80	20
	$[Ru(NH_3)_6]^{3+}$	33				
Ru_{C77}-CYP119(H)	unquenched	200	220	45	85	15
	$[Ru(NH_3)_6]^{3+}$	91				
Ru_{C77}-CYP119($_H$W)	unquenched	130	91	320	75	25
	$[Ru(NH_3)_6]^{3+}$	48				

3.2.3. Ru-P450 transient absorption

We have probed ET in the Ru-P450 systems using single-wavelength transient absorption (TA) spectroscopy. As described in Chapter 2 and illustrated in **Figure 3.9**, both the photosensitizer and P450 heme have strong electronic absorbance in the 390-440 nm region, and the shapes and positions of these electronic transitions are sensitive to metal oxidation state and environment.

As found for Ru^{II}C97-BM3(W), TA traces of the other three mutants in the absence of exogenous quencher reveal bleaching in the 390-440 nm region, consistent with formation and decay of the *Ru(II) excited state; there is no observed formation of electron transfer intermediates. None of the unlabeled proteins show detectable transient absorption features following excitation at 480 nm (data not shown).

P450-BM3 mutants: effect of tryptophan 96

We first compare the tryptophan- and histidine-containing P450-BM3 photochemical systems. As described in Chapter 2, transient absorption features for RuC97-BM3(W) displays complex, multiexponential kinetics in the presence of ET quencher, $[Ru(NH_3)_6]^{3+}$ (**Figure 3.15,** left). In particular, we observed a bleach at 420 nm (the peak of the heme Soret) which persisted for nearly 200 ms; this was indicative of heme oxidation. Additionally, we observed an increase in absorption at 440 nm, which was attributed to the formation of high-valent CII on the millisecond timescale. If heme oxidation occurs in the other mutants, we expect to see similar TA features.

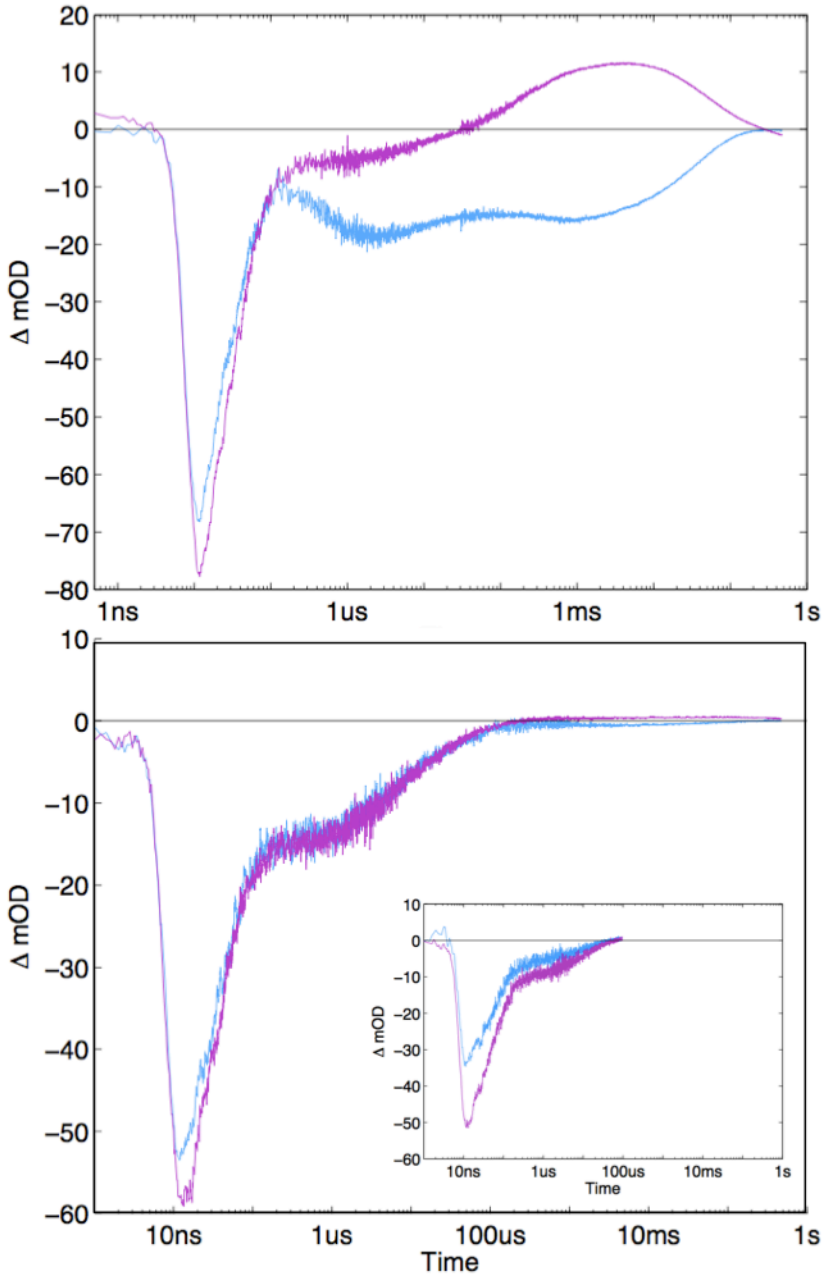

Figure 3.15. Single wavelength TA traces of Ru_{K97C}-$P450_{BM3}$ conjugates in the presence of $[Ru(NH_3)_6]^{3+}$, following excitation at 480 nm. Blue: 420 nm; Purple: 440 nm. **Top**: RuC97–BM3(W). **Bottom**: RuC97–BM3($_W$H). **Inset**: Model complex $[Ru(bpy)_2(Aphen)]^{2+}$ with $[Ru(NH_3)_6]^{3+}$, for comparison.

For the histidine-containing mutant, RuC97–BM3($_{W}$H), TA traces in the presence of $[Ru(NH_3)_6]^{3+}$ are significantly simpler (**Figure 3.15**, right). TA features at all wavelengths examined (390-440 nm) show biphasic decays that return to baseline within 200 μs. There is no persistent bleach at 420 nm past 100 μs, nor is there an increase in absorption at 440 nm at any point in time. The observed features can be explained by a simple reaction scheme involving only the photosensitizer, with no heme oxidation (**Figure 3.16**). Indeed, the TA traces for RuC97–BM3($_{W}$H) are nearly identical to those seen for the free photosensitizer $[Ru(bpy)_2(Aphen)]^{2+}$ with $[Ru(NH_3)_6]^{3+}$ (**Figure 3.15,** inset).

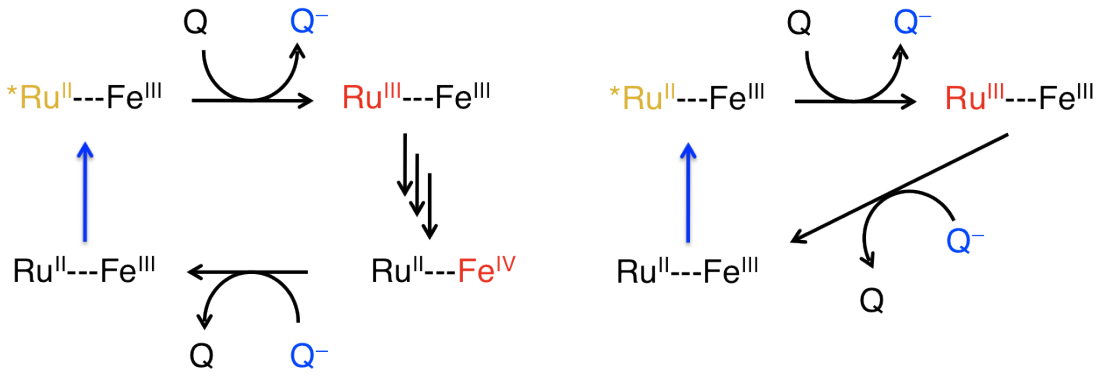

Figure 3.16. Flash-quench schemes. **Left**: Photochemically-generated Ru^{III}_{C97}–BM3(W) oxidizes the BM3(W) heme. Multiple arrows indicate that several processes are required to form the Fe(IV) product. **Right**: Photochemically-generated Ru^{III}_{C97}–BM3($_{W}$H) nonproductively recombines with reduced quencher.

ET reactivity of CYP119 mutants

We have also examined flash-quench of Ru_{C77}-CYP119(H) and Ru_{C77}-CYP119($_{H}$W) in the presence of $[Ru(NH_3)_6]^{3+}$. For Ru_{D77C}-CYP119(H), biphasic kinetics are observed in the 390-440 nm region (**Figure 3.17**). These are nearly identical to those observed for Ru_{C97}-BM3($_{W}$H), and can be explained in a similar $^*Ru^{II} \rightarrow Ru^{III} \rightarrow Ru^{II}$ reaction scheme, with no involvement of the heme center.

TA traces for Ru_{C77}-CYP119($_H$W) are distinct from its histidine-containing counterpart, and can be compared to the tryptophan-containing BM3 mutant. As seen for the functional system Ru_{C97}-BM3(W), there is a small but persistent bleach at 420 nm, and another (even smaller) increase in absorbance at 440 nm on the millisecond timescale. These transient signals are much smaller than for RuC97-BM3(W) (< 5 mOD), but they have similar wavelength profiles, and occur on similar timescales (**Figure 3.17**, inset).

Unfortunately, the small signal amplitudes and poor signal-to-noise ratio make it difficult to extract rate constants for the formation and decay of intermediates in the Ru_{C77}-CYP119($_H$W) system. The ET event of interest is oxidation of the porphyrin to form $Fe^{III}(OH_2)(porphyrin)^{+\bullet}$ species. In Ru_{C97}-BM3(W), this is observed as a pronounced, re-bleaching at 420 nm that reaches completion at ~ 2 μs (see **Figure 3.17**, inset). Additionally, two $Fe^{III}(OH_2)(porphyrin)^{+\bullet}$ species were identified, in addition to the formation of CII. In Ru_{C97}-BM3($_W$H), however, this second bleach not apparent, and cannot be readily distinguished from Ru^{III} formation. The low signal-to-noise ratio at all wavelengths examined also makes it difficult to characterize intermediates (such as multiple $Fe^{III}(OH_2)(porphyrin)^{+\bullet}$ species). Guided by the transient at 440 nm, it may be possible to determine a rate for CII formation. However, without knowing the identity of the preceding species, it is difficult to draw conclusions as to the molecular nature of that event.

From the current TA data, we cannot quantitatively determine if the small amplitudes are primarily a result of decreased heme oxidation rate, or a decrease in yield by competition with nonproductive ET processes. It appears that the maximum signal amplitude at 440 nm occurs at 4 ms for Ru_{C97}-BM3(W) (**Figure 3.17** inset, red trace), while the maximum signal for Ru_{C77}-CYP119($_H$W) is seen at

30 ms; this suggests that a difference in rate of CII formation may account for some of the discrepancy.

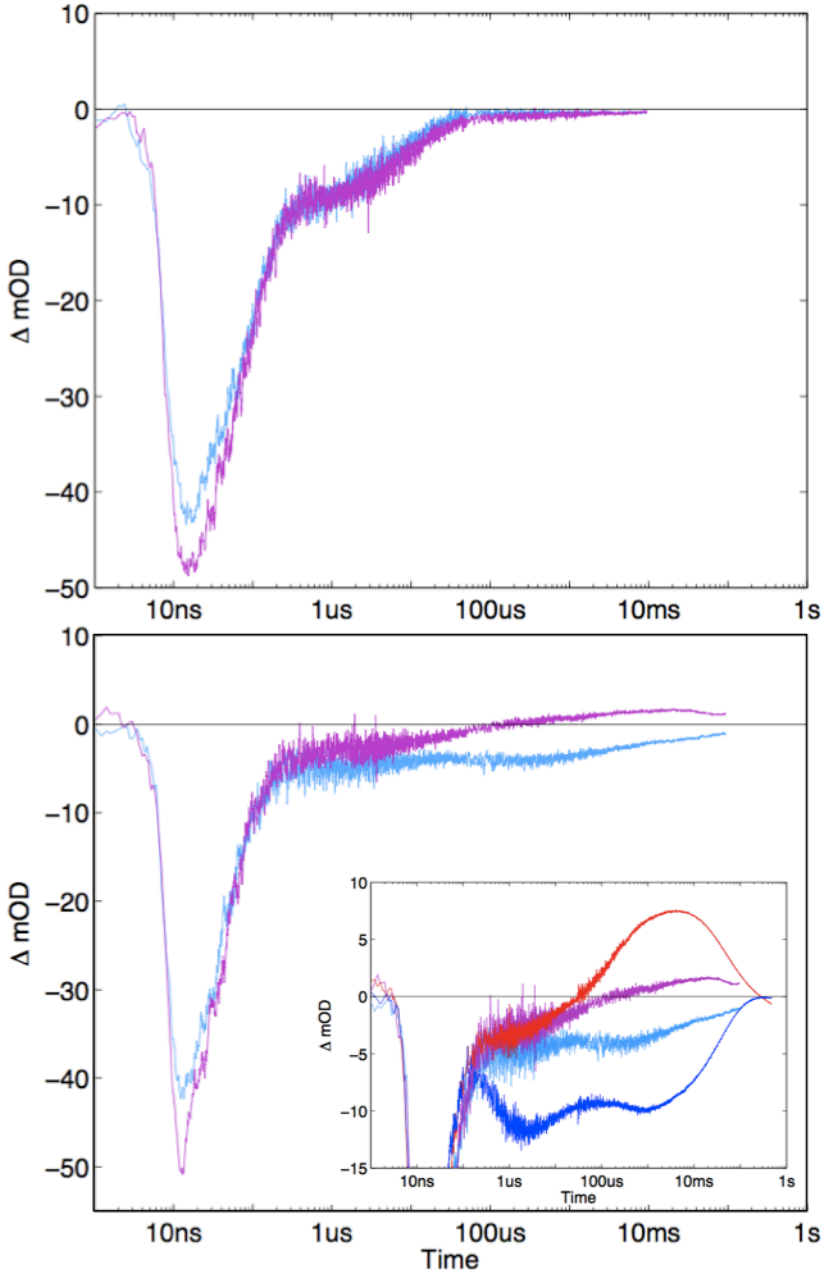

Figure 3.17. Single wavelength transient absorption traces of Ru-CYP119 conjugates in the presence of $[Ru(NH_3)_6]^{3+}$, following excitation at 480 nm. Light blue: 420 nm; purple: 440 nm. **Left**: Ru_{C77}-CYP119(H). **Right**: Ru_{C77}-CYP119($_H$W). **Inset**: Overlay of TA from Ru_{C97}-BM3(W) scaled to the magnitude of the $^*Ru^{II}$ bleach: 440 nm (red), 420 nm (dark blue).

Temperature dependence

The flash-quench transient absorption studies for Ru-CYP119 conjugates also were conducted at elevated temperature (40 °C).

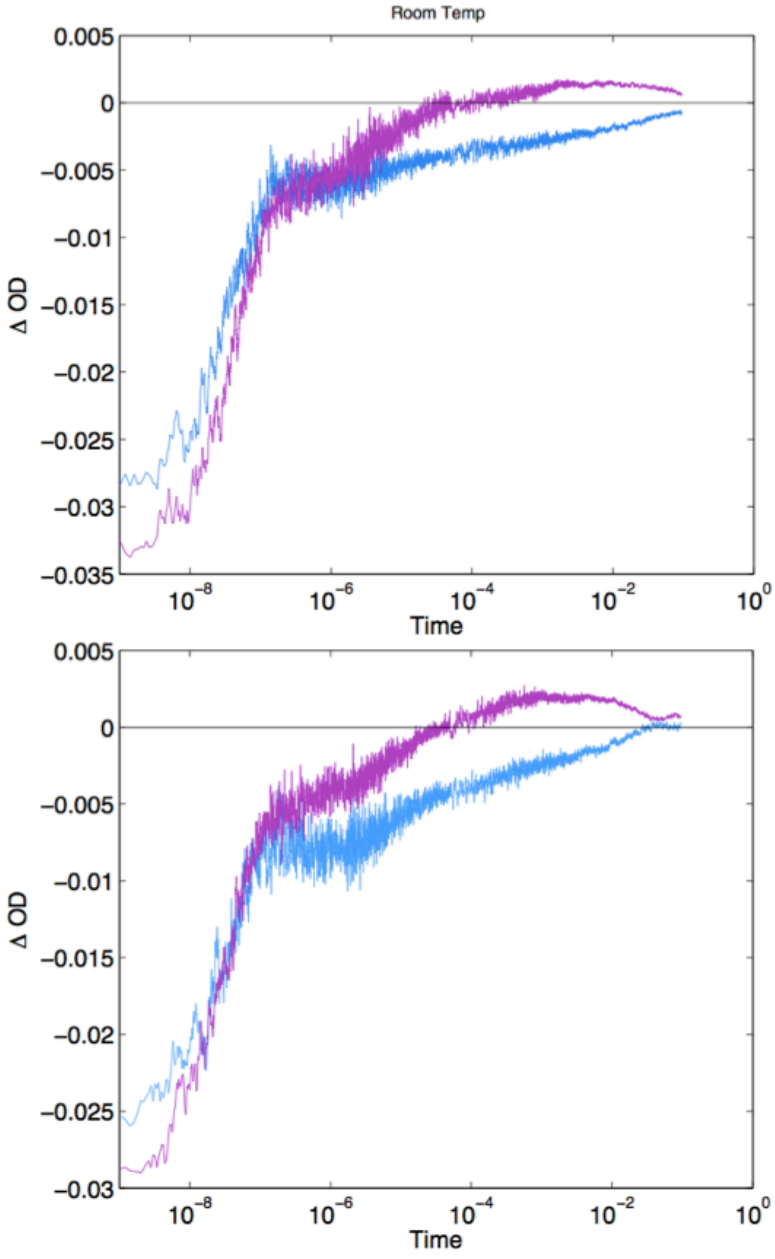

Figure 3.18. TA data of Ru_{C77}-CYP119($_{H}$W) at variable temperature. 420 nm (blue) and 440 nm (purple). **Top**: Room temperature. **Bottom**: 40 °C.

The magnitudes of TA features are slightly larger at a temperature of 40 °C, however, the increase is not sufficient to distinguish ET quenching of the photosensitizer (Ru^{III} formation) from porphyrin oxidation. While the CYP119 enzyme is stable over temperatures of 80 °C, the $[Ru(NH_3)_6]^{3+}$ quencher noticeably decomposes at temperatures of 70 °C.

Search for the transient tryptophan radical

Direct observation of the oxidized tryptophan intermediate would provide more tangible support for a hopping mechanism. Tryptophan radical cation ($W^{\bullet+}$) and neutral radical ($W^{\bullet}$) species absorb in the visible region (**Figure 3.19**), with approximate extinction coefficients of $\varepsilon(\lambda_{max}$: 560 nm) = 3000 M^{-1} cm^{-1} and $\varepsilon(\lambda_{max}$: 510 nm) = 2300 M^{-1} cm^{-1}, respectively.[17] We examined TA in the 500-600 nm region to see if such an intermediate could be identified in the Ru_{C97}-BM3(W) and Ru_{C77}-CYP119($_H$W) systems (see Appendix C for more details). Unfortunately, we are unable to identify the formation of these species.

If the rate of tryptophan oxidation is slower than its reduction via ET from the porphyrin, we would not anticipate accumulation of $W^{\bullet+}$/$W^{\bullet}$ species. It is also possible that any tryptophan radical transients are obscured by changes in absorbance of the ruthenium photosensitizer (*Ru^{II}, Ru^{III}, < 30 μs) and the P450 Q-bands. In particular, the latter fully overlap with the ($W^{\bullet+}$) and ($W^{\bullet}$) absorbances, but with much higher extinction coefficients: $\varepsilon(\lambda_{max}$: 536 nm) = 9800 M^{-1} cm^{-1} and $\varepsilon(\lambda_{max}$: 568 nm) = 9570 M^{-1} cm^{-1}.

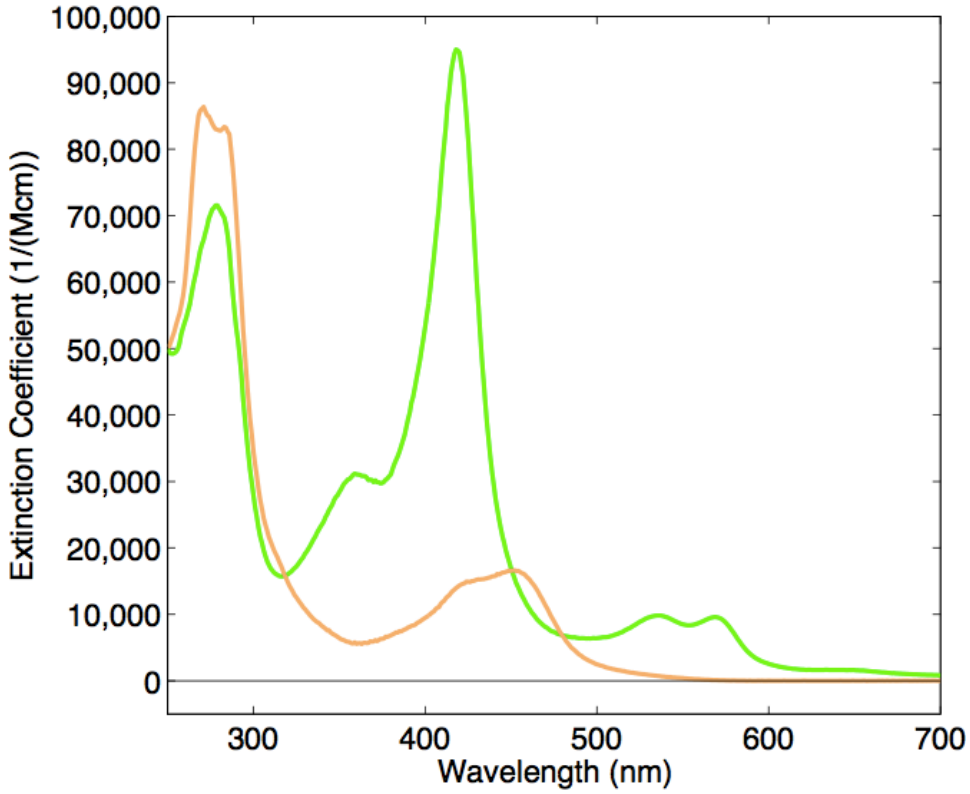

Figure 3.19. UV-visible absorbance spectra P450 and Ru photosensitizer. $[Ru(bpy)_2(IAphen)]^{2+}$ (orange) and Ru_{C97}-BM3(W) (green), assuming ε(418 nm, P450 BM3)=95,000 M^{-1} cm^{-1},[18] ε(450 nm, $[Ru(bpy)_2(Aphen)]^{2+}$)=15,000 M^{-1} cm^{-1}.[19]

3.3. Discussion

We expressed and characterized a P450 BM3 mutant in which W96 has been replaced by histidine: C97–BM3($_W$H). This point mutation does not affect the structure of this enzyme, as examined by crystal structure analysis and comparison to wild-type P450 BM3. The Ru_{C97}–BM3($_W$H) conjugate system supports flash-quench to form Ru^{III} oxidants, as observed by TA. There is no observable formation of oxidized P450 intermediates, such as porphyrin cation radicals and CII species. These results suggest that in our original construct, Ru_{C97}–BM3(W), the W96 residue is transiently oxidized in a multi-step electron transfer reaction; this accelerates the ET event and allows accumulation of oxidized heme species. In the absence of W96, the rate of single-step heme oxidation may be unable to

compete with bimolecular recombination with reduced quencher ($\tau \sim 25$ μs). We cannot conclusively rule out the possibility that W96 acts as a sink for some portion of the photogenerated holes. However, our TA data suggest that the ET rate advantage conveyed by W96 is a more important pathway.

We also generated a thermostable CYP119 Ru-P450 conjugate in which the photosensitizer-tethering point mimics that of the Ru-BM3 system. Flash-quench of Ru_{C77}-CYP119(H) generates Ru^{III}; however, no heme oxidation is observed. TA data are nearly identical to those of the histidine-containing P450 BM3 system, Ru_{C97}–BM3($_{W}$H). The H76W mutation (Ru_{C77}-CYP119($_{H}$W)) is sufficient to allow observation of at least a small amount of oxidized heme species. This observation also supports involvement of tryptophan in photochemical oxidation. We suggest that this residue (BM3(W) or CYP119($_{H}$W)) provides a relay station for accelerated multistep ET.

Many challenges still face this analysis. The small signal amplitudes and poor signal-to-noise of Ru_{C77}-CYP119($_{H}$W) transient features make it difficult to extract rate constants for the formation and decay of ET intermediates, particularly the formation of the initial porphyrin radical. The tryptophan side chain is significantly bulkier than that of histidine, and it is possible that the H76W mutation has caused a larger structural change which makes ET more difficult. Crystallographic characterization of the CYP119 mutants would be helpful for identifying or ruling out structural disruptions; these efforts are ongoing.

Another possibility for the small observed yield of heme oxidation is that the $W^{+\bullet}$/W or $por^{+\bullet}$/por reduction potentials in CYP119 may be different from those in P450 BM3. Unfortunately, the reactivity of these oxidized intermediates precludes experimental determination of reduction potentials.

Final thoughts and avenues for future work

One of the main objectives of developing the photochemical system in CYP119 was to establish a more robust framework in which we could chemically generate CII, followed by flash-quench to generate the active species, CI. By identifying the importance of the tryptophan residue in accelerating ET and/or improving ET yield, we have been able to observe the first indication of photochemical ET in CYP119. However, if we wish to observe photochemical generation of CI, we must make significant improvements on two fronts.

First, we must improve the rate and yield of heme oxidation in CYP119. This can be facilitated by a better understanding of the complex factors affecting ET. Crystallization of CYP119 mutants can help elucidate whether other structural features affect the hopping pathway between photosensitizer and heme. The photosensitizer potential can be tuned and the linker-length shortened by synthetic modification, the conjugation-site can be changed, and other mutations may be made to the protein scaffold in order to optimize ET. This knowledge will be useful not only in developing these specific P450 systems, but in using the intramolecular flash-quench method to generate oxidized intermediates in other biological systems.

Second, we must investigate the generation of CII by *chemical* means. Compound ES (CII with an additional hole localized on an amino acid side chain) has been generated in high yield and characterized in CYP158 from *Streptomyces coelicolor*.[5] Similar investigation must be accomplished for CYP119, focusing efforts on the generation of a *singly* oxidized CII species. Chemical oxidation of Ru-P450 conjugates will be further complicated by the redox nature of the photosensitizer

itself. All of these issues must be carefully examined and optimized for before we can expect to observe the second oxidative electron transfer.

3.4. Conclusions

The single W96H mutation in P450 BM3 completely eliminates photochemical heme oxidation in Ru-P450 conjugates. The P450 structure and stability appear unaffected by this mutation, suggesting that W96 is indeed involved in the electron transfer event. Flash-quench oxidation of the histidine-containing Ru_{C77}-CYP119(H) conjugate was unsuccessful, and the single H76W mutation was sufficient to restore a small amount of electron transfer with the heme active site. While we are unable to directly detect formation of a tryptophan radical species, the observation that heme oxidation occurs *only* in the presence of an intervening tryptophan for both P450-BM3 and CYP119 systems strongly implicates this residue as a redox intermediate in multistep electron transfer. We will analyze the kinetics of electron hopping in Chapter 4.

3.5. Acknowledgments

I would like to specifically acknowledge Eric Brustad for assistance in protein crystallization and structure determination. Jay Winkler and Jeff Warren provided helpful discussions.

3.6. Materials and Methods

Materials

Buffer salts were obtained from J.T. Baker. Dicyclohexylcarbodiimide (DCC), iodoacetic acid, and 5-amino-1,10-phenanthroline were obtained from Sigma Aldrich. $[Ru(2,2'\text{-bipyridine})_2]Cl_2$ and $[Ru(NH_3)_6]Cl_3$ were obtained from Strem

Chemicals. All chemicals were used as received with no further purification. Solutions were prepared using 18 MΩcm water unless otherwise noted. Mutagenesis primers were obtained from Operon.

Procedures

A detailed description of experimental protocols can be found in Appendix B. A brief description of the procedures is given below, highlighting any deviations from the general protocol. All figures of protein structures were made in PyMol graphics software for Mac.

3.6.1. Photosensitizer Synthesis

Synthesis

This photosensitizer was synthesized according to published procedures. Briefly, iodoacetic anhydride was formed by addition of N,N'-Dicyclohexylcarbodiimide (DCC) to a solution of iodoacetic acid in ethyl acetate. Following removal of urea by filtration and evaporation to dryness, the iodoacetic anhydride in acetonitrile was added to a solution of 5-amino-1,10-phenanthroline in acetonitrile and stirred overnight at room temperature. Solid product (5-iodoacetamido-1,10-phenanthroline (IAphen)) was refluxed with $Ru(bpy)_2Cl_2$ in methanol for 3 hours; a color change from purple to red is observed. After cooling and filtration, product can be precipitated by addition of concentrated aqueous NH_4PF_6. Alternatively, the compound can be concentrated and redissolved in water without further purification. The starting material impurities do not interact with P450, and do not appear to impact the labeling process.

Characterization

The photosensitizer was characterized by nuclear magnetic resonance (NMR), steady-state luminescence, and transient luminescence and absorption.

3.6.2. Protein mutagenesis, expression, and purification

Plasmid

The recombinant P450-BM3 heme domain, consisting of the first 463 residues with an N-terminal 6-histidine tag, was obtained courtesy of Professor Andrew Udit (Occidental College, Los Angeles California), within the pCWori^{+} vector (also containing genes for ampicillin resistance and IPTG induction). Recombinant CYP119 with an N-terminal 6-histidine tag was obtained courtesy of Professor Paul Ortiz de Montellano (University of California, San Francisco), also within the pCWori^{+} vector.

Mutagenesis

Qiagen Quik-Change site-directed mutagenesis was used to generate the desired P450 mutants. The mutagenesis primers (forward, 5'-3') were: BM3-W96H: GGACGCATGAAAAAAATCATTGCAAAGCGCATAATATC; CYP119-D77C: GATCCCCCTCTCCATTGTGAGTTAAGATCAATGTCAGC and CYP119-(D77C)H76W: CCTCAGATCCCCCTCTCTGGTGTGAGTTAAGATCAATGTC

Overexpression in E. coli.

The P450 mutants BM3-C62A/C156S/K97C/W96H ($_{C97}$BM3($_{W}$H), CYP119-D77C ($_{C77}$CYP119(H)), and CYP119-D77C/H76W ($_{C77}$CYP119($_{H}$W)) were overexpressed in the BL21-DE3 strain of *E. coli*. Briefly, overnight LB cultures were used to inoculate 1x TB (for P450 BM3) or 2x TB (for CYP 119) induction cultures. After

approximately three hours at 37 °C (OD_{600} ~ 1) the temperature was lowered to 30 °C, expression was induced with IPTG and α-aminolevulenic acid was added. After expression for 24 or 40 hours (for P450 BM3 and CYP119, respectively), cells were harvested by centrifugation and stored at -80 °C.

P450 enzymes were extracted by sonication, centrifuged to pellet cellular debris, and purified by Ni immobilized metal affinity chromatography (IMAC) . Enzymes were further purified by anion-exchange FPLC and gel filtration. Dithiothreitol (DTT) was added to reduce intermolecular disulfide bonds for samples not intended for immediate use. 40% glycerol was added to these samples, which were flash-frozen in liquid nitrogen and stored at -80 °C.

P450 mutants were characterized by UV-vis spectroscopy and mass spectrometry.

3.6.3. Conjugation to Ru-photosensitizer

Briefly, approximately three-fold excess of $Ru^{II}(bpy)_2$(IAphen) was added to a ~10 μM P450 solution in 20 mM Tris buffer, pH 8 (buffer-exchanged to remove DTT). The reaction solution shaken gently for ~4 hours at 4 °C in the dark, followed by desalting to remove excess photosensitizer, and purification of Ru-labeled and unlabeled enzymes by anion exchange chromatography on a MonoQ or HiPrepQ FPLC column.

Successful conjugation and separation of Ru-P450 was verified by UV-vis, mass spectrometry, and fluorometry.

3.6.4. Crystallization and structure determination

Crystals of $_{C97}$-BM3($_{W}$H) were obtained by the sitting-drop vapor diffusion method: 10 mg/mL $_{C97}$-BM3($_{W}$H) in 10 mM Tris, 10 mM sodium chloride, pH 7.4

was mixed with a crystallization well solution of 0.1 M sodium cacodylate pH 6.0, 0.14 M $MgCl_2$, 18% PEG 3350 in a 1:1 ratio (v/v). Crystal formation could be observed within a period of 30 minutes, but were allowed to form over 24 hours at 20 °C, and were flash-frozen directly from solution. X-ray diffraction data were collected at Stanford Synchrotron Radiation Laboratory Beamline 12-2.

3.6.5. Preparation of laser samples

Laser samples were composed of ~10 μM Ru-P450 conjugate, with and without oxidative quencher (17 mM $[Ru(NH_3)_6]Cl_3$) in buffered solution (pH 8: 50 mM sodium borate or 50 mM Tris); additionally, each buffer contained sodium chloride to prevent precipitation. Samples were placed in a high-vacuum four-sided quartz cuvette with high-vacuum Teflon valve, equipped with a small stir bar. Deoxygenation was achieved via gentle pump-backfill cycles with argon.

For acquisition of time-resolved fluorescence and transient absorption data, samples were excited with 10 ns laser pulses at 480 nm. Luminescence decays were monitored at 630 nm. Single wavelength transient absorption (TA) kinetics were monitored every 10 nm from 390-440 nm, averaging ~500 shots per wavelength. Data from five separate timescales (2 μs, 40 μs, 400 μs, 10 ms, and 500 ms) were collected, log-compressed, and spliced together to produce full kinetics traces. See Appendix D for log-compression and splicing scripts in Matlab.

3.7. References

(1) Ener, M. E.; Lee, Y.-T.; Winkler, J. R.; Gray, H. B.; Cheruzel, L. Photooxidation of Cytochrome P450-BM3. *Proc. Natl. Acad. Sci.* **2010**, *107*, 18783–18786.

(2) Rittle, J.; Green, M. T. Cytochrome P450 Compound I: Capture, Characterization, and C-H Bond Activation Kinetics. *Science* **2010**, *330*, 933–937.

(3) Davydov, R.; Makris, T. M.; Kofman, V.; Werst, D. E.; Sligar, S. G.; Hoffman, B. M. Hydroxylation of Camphor by Reduced Oxy-Cytochrome P450cam: Mechanistic Implications of EPR and ENDOR Studies of Catalytic Intermediates in Native and Mutant Enzymes. *J. Am. Chem. Soc.* **2001**, *123*, 1403–1415.

(4) Green, M. T.; Dawson, J. H.; Gray, H. B. Oxoiron(IV) in Chloroperoxidase Compound II Is Basic: Implications for P450 Chemistry. *Science* **2004**, *304*, 1653–1656.

(5) Yosca, T. H.; Rittle, J.; Krest, C. M.; Onderko, E. L.; Silakov, A.; Calixto, J. C.; Behan, R. K.; Green, M. T. Iron(IV)hydroxide pKa and the Role of Thiolate Ligation in C-H Bond Activation by Cytochrome P450. *Science* **2013**, *15*, 825–829.

(6) Krest, C. M.; Onderko, E. L.; Yosca, T. H.; Calixto, J. C.; Karp, R. F.; Livada, J.; Rittle, J.; Green, M. T. Reactive Intermediates in Cytochrome P450 Catalysis. *J. Biol. Chem.* **2013**, *288*, 17074–17081.

(7) Hamachi, I.; Tsukiji, S.; Shinkai, S.; Oishi, S. Direct Observation of the Ferric-Porphyrin Cation Radical as an Intermediate in the Phototriggered Oxidation of Ferric- to Ferryl-Heme Tethered to $Ru(bpy)_3$ in Reconstituted Materials. *J. Am. Chem. Soc.* **1999**, *121*, 5500–5506.

(8) Shih, C.; Museth, A. K.; Abrahamsson, M.; Blanco-Rodríguez, A. M.; Di Bilio, A. J.; Sudhamsu, J.; Crane, B. R.; Ronayne, K. L.; Towrie, M.; Vlček, Jr., A.; Richards, J. H.; Winkler, J. R.; Gray, H. B. Tryptophan-Accelerated Electron Flow Through Proteins. *Science* **2008**, *320*, 1760–1762.

(9) Warren, J. J.; Ener, M. E.; Vlček Jr., A.; Winkler, J. R.; Gray, H. B. Electron Hopping through Proteins. *Coord. Chem. Rev.* **2012**, *256*, 2478–2487.

(10) Warren, J. J.; Herrera, N.; Hill, M. G.; Winkler, J. R.; Gray, H. B. Electron Flow through Nitrotyrosinate in Pseudomonas Aeruginosa Azurin. *J. Am. Chem. Soc.* **2013**, *135*, 11151–11158.

(11) Munro, A. W.; Malarkey, K.; McKnight, J.; Thomson, A. J.; Kelly, S. M.; Price, N. C.; Lindsay, J. G.; Coggins, J. R.; Miles, J. S. The Role of Tryptophan 97 of Cytochrome P450 BM3 from Bacillus Megaterium in Catalytic Function. Evidence against the "Covalent Switching" Hypothesis of P-450 Electron Transfer. *Biochem. J.* **1994**, *303*, 423–428.

(12) Huvaere, K.; Skibsted, L. H. Light-Induced Oxidation of Tryptophan and Histidine. Reactivity of Aromatic N-Heterocycles toward Triplet-Excited Flavins. *J. Am. Chem. Soc.* **2009**, *131*, 8049–8060.

(13) Creutz, C.; Chou, M.; Netzel, T. L.; Okumura, M.; Sutin, N. Lifetimes, Spectra, and Quenching of the Excited States of Polypyridine Complexes of Iron(II), Ruthenium(II), and Osmium(II). *J. Am. Chem. Soc.* **1980**, *102*, 1309–1319.

(14) Sutin, N.; Creutz, C. Properties and Reactivities of the Luminescent Excited States of Polypyridine Complexes of Ruthenium(II) and Osmium(II). In *Inorganic and Organometallic Photochemistry*; Advances in Chemistry; American Chemical Society: Washington, DC, 1978; Vol. 1.

(15) Raner, G.; Thompson, J.; Haddy, A.; Tangham, V.; Bynum, N.; Reddy, R.; Ballou, D.; Dawson, J. Spectroscopic Investigations of Cytochrome P450(BM3)-F87G of Intermediates in the Reaction with Surrogate Oxygen Atom Donors. *J. Inorg. Biochem.* **2006**, *100*, 2045–2053.

(16) Spolitak, T.; Dawson, J.; Ballou, D. Rapid Kinetic Investigations of Peracid Oxidation of Ferric Cytochrome P450cam: Nature and Possible Function of Compound ES. *J. Inorg. Biochem.* **2006**, *100*, 2034–2044.

(17) Solar, S.; Getoff, N.; Surdhar, P. S.; Armstrong, D. A.; Singh, A. Oxidation of Tryptophan Ad N-Methylindole by N3*, Br2*-, and (SCN)2*- Radicals in Light- and Heavy-Water Solutions: A Pulse Radiolysis Study. *J. Phys. Chem.* **1991**, *95*, 3639–3643.

(18) Quaroni, L. G.; Seward, H. E.; McLean, K. J.; Girvan, H. M.; Ost, T. W. B.; Noble, M. A.; Kelly, S. M.; Price, N. C.; Cheesman, M. R.; Smith, W. E.; Munro, A. W. Interaction of Nitric Oxide with Cytochrome P450BM3. *Biochemistry* **2004**, *43*, 16416–16431.

(19) Castellano, F. N.; Dattelbaum, J. D.; Lakowicz, J. R. Long-Lifetime Ru(II) Complexes as Labeling Reagents for Sulfhydryl Groups. *Anal. Biochem.* **1998**, *255*, 165–170.